Master's Thesis

Biodegradable, electro-active chitin nanofiber films

for flexible piezoelectric transducers

Kyungtae Kim

Department of Energy Engineering

(Battery Science and Technology)

Graduate School of UNIST

2018

Biodegradable, electro-active chitin nanofiber films for flexible piezoelectric transducers

Kyungtae Kim

Department of Energy Engineering

(Battery Science and Technology)

Graduate School of UNIST

Biodegradable, electro-active chitin nanofiber films for flexible piezoelectric transducers

A thesis/dissertation

submitted to the Graduate School of UNIST

in partial fulfillment of the

requirements for the degree of

Master of Science

Kyungtae Kim

06/05/2018 of submission
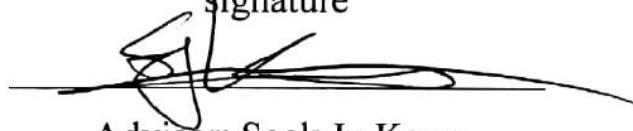
Approved by

Advisor

Seok Ju Kang

Biodegradable, electro-active chitin nanofiber films for flexible piezoelectric transducers

Kyungtae Kim

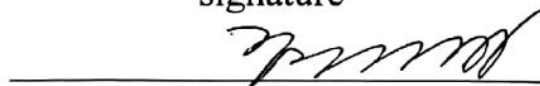This certifies that the thesis/dissertation of Kyungtae Kim is approved.
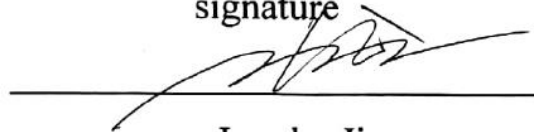
06/05/2018

signature

Advisor: Seok Ju Kang

signature

Hyunhyub Ko

signature

Jungho Jin

4

Contents

Abstract

Since the conventional fluorine-based electro-active polymers release toxic residues into the environment during their syntheses and decomposition processes, eco-friendly piezoelectric polymers are urgently demanded in the field of energy-related soft materials. Here, we derive a high-performance biodegradable chitin polymer from squid pen material and demonstrate its utility as a flexible piezoelectric material. The readily controlled ferroelectric chitin film confers excellent piezoelectricity under external mechanical pressure, resulting in comparable performance with that of conventional fluorine-based piezoelectric polymers. In particular, the sufficient piezoelectric behavior in chitin film allows us to not only realize a high-fidelity paper-type speaker and microphone that operates over a wide frequency range without significantly deteriorating the input and output sounds but also demonstrate transparent speaker consisting of AgNWs electrodes onto freestanding chitin film which also enables to resemble the original sound. Finally, the biodegradable chitin polymer can be successfully dissolved by chitinase enzyme within eight days without any toxic residues remained.

List of figures

glass (blue line), and PI (orange line). The transmittance of freestanding chitin film is 92%. b) Stress-strain curves of chitin freestanding film (red line) and PVDF film (blue line). The extension rate is 0.1 mm/min. Inset table shows the Young's modulus and tensile strength of 35 μm thick chitin film and 80 μm thick PVDF film.

Figure 1.11 2D WAXS pattern of the freestanding chitin film. The three intensified Debye–Scherrer reflections are assigned to (010), (002) and (100) planes.

Figure 1.12 Photographic image of freestanding chitin film with Ag electrode (100 nm) on both sides.

Figure 1.13 Plots of a) output current density (red dotted line) and voltage (blue dotted line) versus input pressure. Inset shows the linear sensitivity of the current density and voltage in the low-pressure regime (< 10 kPa). b) Output current density from α- (red) and β- (blue) chitin film under the consecutive normal pressure of 98 kPa.

Figure 1.14 Piezoelectric characteristics of chitin film as a function of external load resistance. a) Output voltage, current density, and b) power density of chitin films with elevating external load from 10^3 to 10^9 Ω by using the vertical loading pressure of 100 kPa.

Figure 1.15 Mechanical durability of the freestanding chitin film over 5,000 times of cyclic pushing motion (100 kPa) and the corresponding output voltage signals.

Figure 1.16 a) Output current densities and b) voltage of the freestanding chitin film under the bending stimuli motion.

Figure 2.1 Digital photographic image of the chitin acoustic actuator ((4 x 6) cm^2) with Ag electrodes on both sides.

Figure 2.2 The chitin speaker electrical circuit consisting of sound source, amplifier, and piezoelectric chitin speaker.

Figure 2.3 Sound pressure level (SPL) spectrum of chitin speaker in the frequency range of 300–20000 Hz.

Figure 2.4 Fast Fourier transform (FFT) spectra of time-dependent piezoelectric voltage signals.

Figure 2.5 a) Schematic illustrations of the piezoelectric chitin transducer b) The short-time Fourier transform (STFT) spectrograms from the analysis of voltage variations of the original sound source, chitin speaker, and chitin microphone based on the playing music with 'Paganini Caprice NO. 24'.

Figure 2.6 STFT patterns of a) the original sound and b) chitin speaker with 'Paganini

Caprice NO. 24'. c) The difference of STFT patterns between the original sound and the STFT pattern of the chitin speaker (synchronization of 70%). The blue color indicates the difference between two images.

Figure 2.7 Digital photograph of the transparent chitin speaker sandwiched between two AgNWs electrodes.

Figure 2.8 a) Transmittance spectra of freestanding chitin film with (blue line) and without (red line) AgNWs electrodes on both sides. b) STFT signals of the transparent chitin speaker, verifying the high-quality sound performance of the transparent chitin speaker.

Figure 2.9 Series photographs and schematic illustrations of corresponding stages of biodegradation process in chitinase solution (1 UN/10ml).

Figure 2.10 Plots of the weight loss of the chitin film as a function of time in chitinase solution (1 UN/10ml).

Figure 2.11 A digital photograph of biodegradation of the chitin film by chitinase solution a) 2 UN/10ml, b) 3 UN/10ml, c) 4 UN/10ml, and d) 5 UN/10ml as time advanced.

Figure 2.12 a) Schematic illustrations of home-built DEMS system. b) The consecutively measured CO_2 signals of chitin film in chitinase solution. The CO_2 evolution is detected after 18 hours and monotonically increased until the end of the measurement. The inset shows a photographic image of chitin film immersed in chitinase solution.

List of tables

Table 1 Lattice parameters and calculated spontaneous polarizations of the optimized crystal structures (in the spontaneous polarization calculations, the lattice vectors b and c were oriented along the y- and z-axis, respectively).

Chapter 1

1. Piezoelectricity for freestanding β-chitin nanofiber films

1.1 Introduction of piezoelectricity

Since the direct piezoelectric effect was discovered in 1880 by Pierre Curie and Jacques Curie[1], many piezoelectric materials of inorganic piezoelectric ceramics and organic piezoelectric polymers have been demanded for a variety of energy-related technology such as energy-harvesting devices, pressure sensors, flexible electronics and artificial skins[2-5]. The basic concept of piezoelectricity is the generation of electric charge when the material deformation by applying mechanical stress. The piezoelectric effect has two types, direct piezoelectric effect and reverse piezoelectric effect. First, direct piezoelectric effect is the electric signal produces by mechanical deformation as above mentioned, and the reverse piezoelectric effect is the sound vibration produces by applying electric voltage in Figure 1.1.
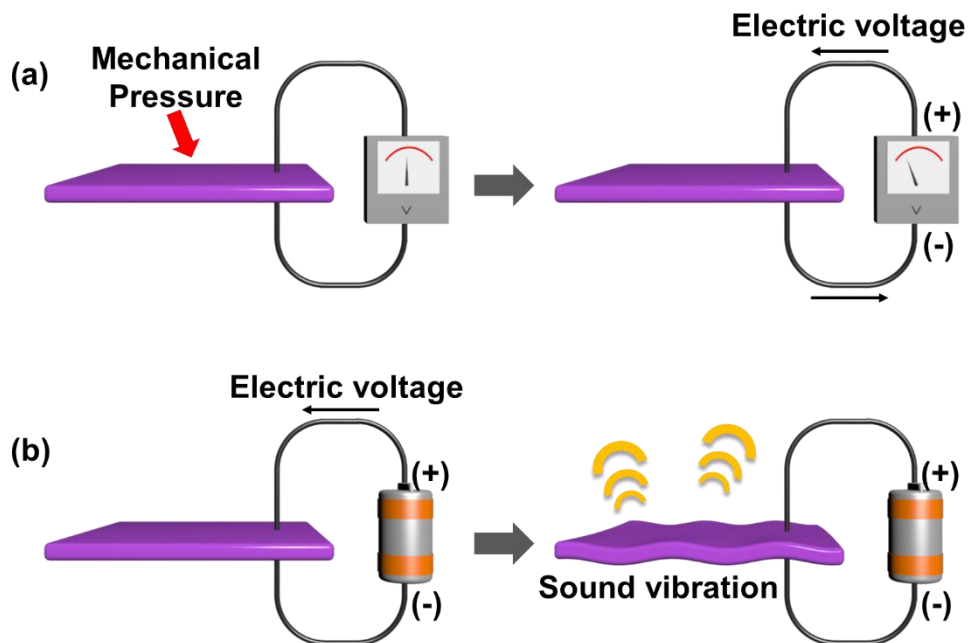

Figure 1.1 The schematic illustrations of the basic concept of a) direct piezoelectric effect and b) reverse piezoelectric effect.

1.2 Piezoelectric materials` research trends and problem

The most representative piezoelectric materials providing stable polarization are inorganic $Pb(Zr_xTi_{1-x})O_3$ (PZT), $BaTiO_3$, and $ZnSnO_3$, where the asymmetric atomic arrangement in the crystals accomplished by high voltage poling plays a fundamental role in managing the response to external pressure.[6] However, these ceramic materials are far from being implanted on modern-day flexible electronics due to their strong rigidity. Thus, it is necessary to explore new, soft-type piezoelectric materials for satisfying the pliable requirements of soft electronics.[7-8] Among them, fluorine-based polymer such as poly(vinylidene fluoride) (PVDF)[9-11], poly(vinylidene fluoride-co-trifluoroethylene) (PVDF-TrFE)[12-13] and poly(vinylidene fluoride-co-trifluoroethlyene-co-chlorotrifluoro ethylene) (PVDF-TrFE-CTFE)[14], have attracted great interest as flexible piezoelectric materials because they are strongly polarized under pressure due to the negatively charged fluorine atoms and positively charged hydrogen atoms in the chain backbones of these polymers. The piezoelectric output responses of these piezoelectric fluorine-based polymers have been developed by crystal orientation control[15], blending with inorganic piezoelectric materials and conductive carbon[16], and electrospinning fiber alignment.[17] Although the development and attention for piezoelectric fluorine-based polymers, the most serious drawback is the formation of toxic gases such as hydrogen fluoride (HF) during degradation or heating process.[18-19] In recent years, piezoelectric biopolymer such as polysaccharides (e.g., chitin[20-21] and cellulose[22-24]) and proteins (e.g., silk[25]) have been focused to overcome these drawbacks due to non-toxicity and eco-friendly characteristics in Figure 1.2.[9, 12, 25-26] In particular, chitin is the second most abundant natural polysaccharide that are being produced at 100 billion tons/year[25] and has the piezoelectric properties (due to intrinsic molecular polarization arising from the non-centrosymmetric crystal structure of α- and β-chitin polymorphs). However, the piezoelectricity of chitin material have rarely been studied since the first discovery of piezoelectricity in 1975 by Eiichi Fukada.[20] The lack of fundamental study of the piezoelectricity of chitin may be attributed to low solubility to organic solvent and the limited material processability. These shortages of chitin make it hard to study on the molecular polarization and the feasibility of piezoelectric devices. In recent works, the piezoelectric response of α-chitin from butterfly wing by Valerie et al[27] and the piezoelectric and ferroelectric properties of α-chitin from prawn shell has studied by Ghosh et al.[21]
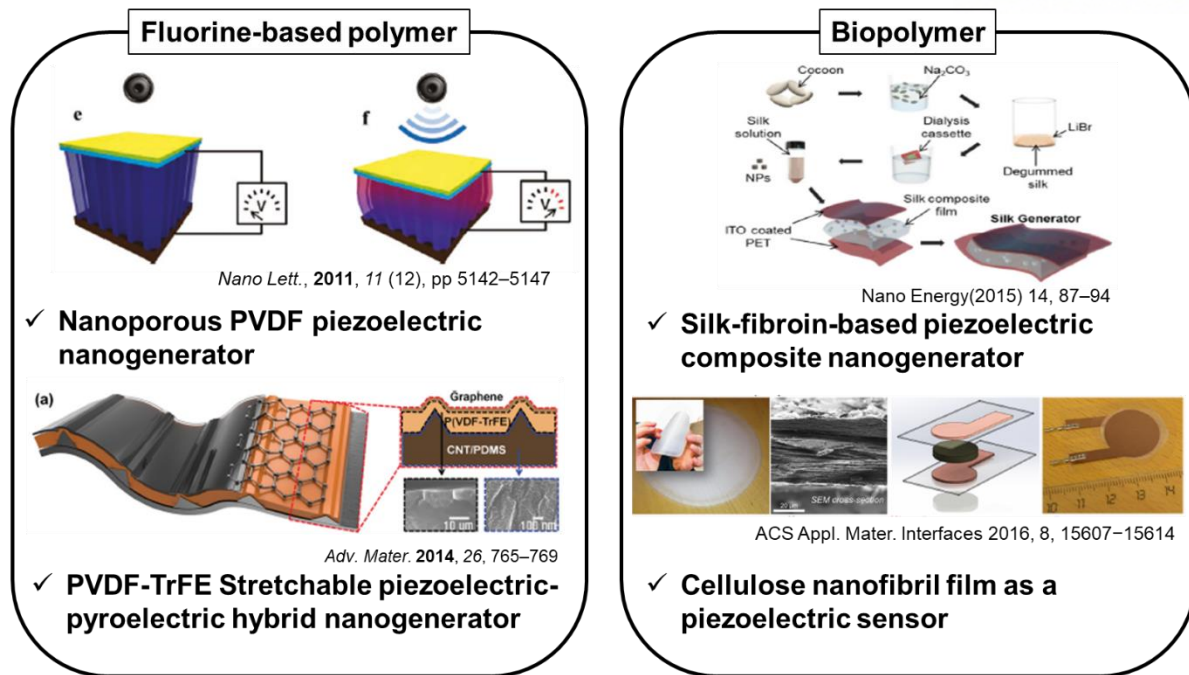
Figure 1.2 Various research works in piezoelectric materials of fluorine-based polymers and biopolymers.

1.3 Chitin crystal phase and ferroelectricity

In this work, we propose a biodegradable, electro-active piezoelectric transducers based on a transparent and flexible β-phase dominant freestanding chitin nanofibers film.[28-29] β-phase dominant crystal structure and void-free characteristics related to the ferroelectric and piezoelectric properties of the chitin nanofibers film. It is well known that chitin exists in two major polymorphs (α-chitin and β-chitin). The α-phase features an antiparallel molecular conformation with dense intermolecular hydrogen bond networks, while the β-phase adopts a parallel conformation due to which the intersheet hydrogen bond network is missing as shown Figure 1.3.[29] Thus, it is expected that such differences in the molecular conformation and chain orientation result in different surface charge along the electric field direction. In order to confirm the crystal phase of chitin thin film with a low roughness of ~7 nm (Figure 1.4a) on the Si wafer substrate, attenuated total reflection Fourier transform infrared (ATR FT-IR) spectroscopy was used. α-chitin shows the split two peaks, 1620 cm^{-1}, which indicate intersheet (C=O…HO) hydrogen bonds and 1660 cm^{-1} which indicates intrasheet

(C=O…HN) hydrogen bonds. β-chitin has the broad peaks at 1630 cm^{-1} with the intrasheet (C=O…HN) hydrogen bonds.[30] The FT-IR peaks of the spin-coated chitin thin film on Si wafer show the broad peaks at 1620, 1630 and 1660 cm^{-1}, which indicate the mixture α- and
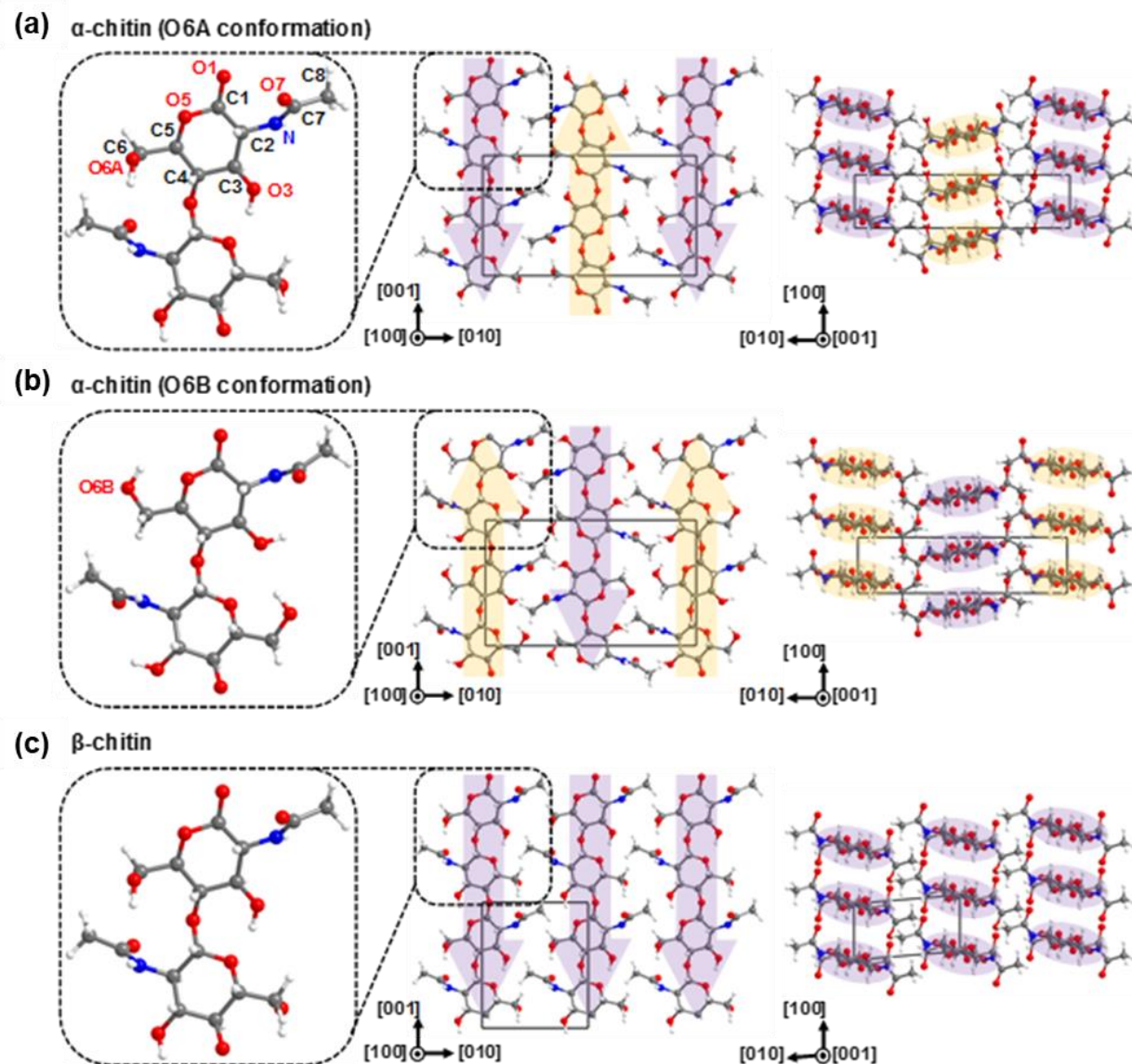
Figure 1.3 Projection views along the [100] and [001] directions of the optimized crystal structures of a) α-chitin with O6A conformation, b) α-chitin with O6B conformation, and c) β-chitin. Magnified images show the molecular structure of β-(1,4)-N-acetyl-D-glucosamine in each crystal structure. Orange and purple arrows indicate the polarization direction of each chitin molecule along [001] and [00$\bar{1}$], respectively. The C, H, N, and O atoms are colored gray, white, blue, and red, respectively.

β-chitin crystal phases in Figure 1.4b, but the calculated ratio of β-phase in chitin film is 70% in Figure 1.5c. The detail chitin crystal phases and polymer chain orientations investigate by 2D grazing-incidence wide-angle X-ray scattering (2D GIWAXS) measurement. 2D GIWAXS patterns in Figure 1.4c displays two distinct peaks on the meridian, which indicate (010) and (100) planes with the reference to the lattice parameter of monoclinic β-chitin (a = 0.485 nm, b = 0.926 nm, c = 1.038 nm and γ = 97.5°).[31] It is noted that the c-axis of the chitin is parallel to the substrate as shown in the inset schematic image of Figure 1.4c.
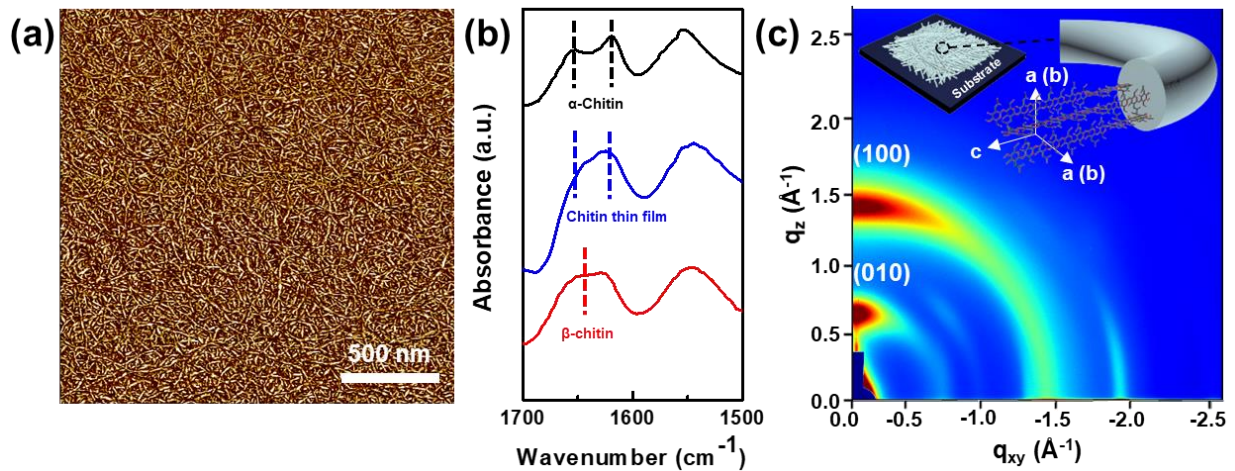
Figure 1.4 a) AFM image of the chitin thin film surface deposited on the highly doped Si wafer. Highly entangled chitin nanofibers appear in the phase contrast image. b) FT–IR absorbance spectra of α-chitin (black line), chitin thin film (blue line), and β-chitin (red line). c) GIXD pattern of 0.2% w/v chitin thin film on Si substrate. The two intensified reflections on the meridian are assigned to (100) and (010) planes. Inset shows the proposed chain orientation in the chitin thin film.
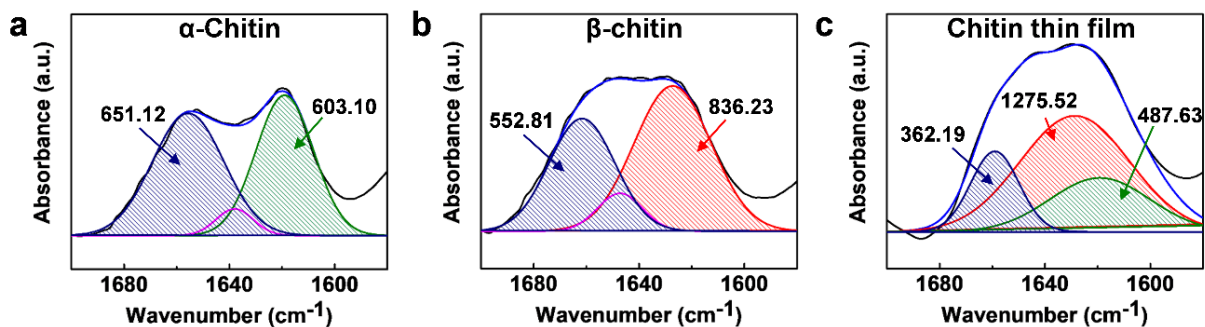
Figure 1.5 FT-IR absorbance spectra (black solid line) and fitted data (blue solid line) of a) α-chitin, b) β-chitin, and c) chitin thin film. The shaded regions of green/blue and red indicate the contribution of α- and β-phase in the fitted data.

To measure the ferroelectric property of β-chitin material, a metal/β-chitin/metal capacitor device was fabricated in the inset schematic image of Figure 1.6a. The ferroelectricity exhibits a spontaneous polarization of electric dipole by the external electric field and reversible polarization-voltage (P-E) hystersis loops with remnant polarization. As shown in Figure 1.6a, the P-E hysteresis loops at various applied voltages exhibit typical ferroelectric hysteresis loop characteristics, which are mainly attributed to the rotation of permanent dipoles with respect to the external electric field in the void-free chitin film. However, the direction mismatch of the applied electric field and the polarization direction with perpendicular to the substrate causes the relatively small polarization values. The dielectric constant (ε_r) of β-chitin thin film is constantly ~4 in 5 kHz-7 MHz (Figure 1.6b).
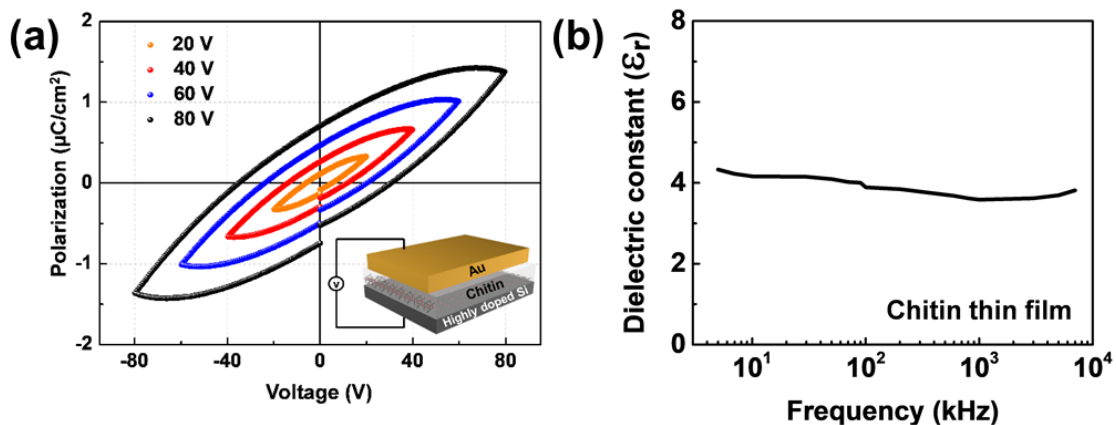
Figure 1.6 a) P–E hysteresis loops of chitin thin film, and (inset) a schematic of the ferroelectric device structure. b) Dielectric constant vs frequency plots of β-rich chitin thin film.

Furthermore, we performed piezoresponse force microscopy (PFM) measurement on β-rich chitin film to confirm the ferroelectric response. The PFM voltage-amplitude characteristics in Figure 1.7 showed the existence of two different polarizations in the chitin film and the slope reveals piezoelectric constant of 3.986 pm/V. This d_{33} value of β-chitin is similar with

that of cellulose materials.[26] In addition, the theoretical polarization values of α- and β-chitin was calculated by density functional theory (DFT) simulation by using The Vienna Ab-initio Simulation Package (VASP).[32-33] While the theoretical spontaneous polarization value of α-chitin is 0 C/m^2 in both case of O6A and O6B conformation, the net polarization value of β-chitin is 1.87 C/m^2 along the [00$\bar{1}$] direction under the boundary conditions in Table 1. However, the experimental polarization value of β-chitin from P-E hysteresis loops is lower than calculated values because the direction of polarization in β-chitin molecules is perpendicular to the electric field direction. It is noted that the ferroelectricity of β-chitin is not only observed from P-E hysteresis loops and PFM measurement using chitin, but also theoretically confirmed by DFT calculation.

Figure 1.7 Plots of PFM voltage-amplitude hysteresis loops of the β-rich chitin thin film. The calculated d_{33} value from PFM is 3.986 pm/V.

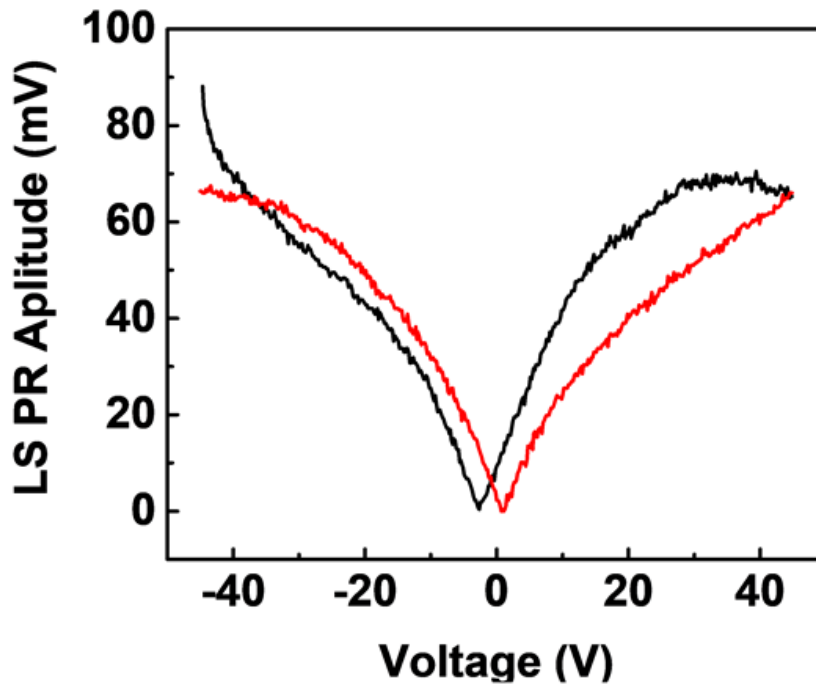|	α-chitin (O6A conformation)	α-chitin (O6B conformation)	β-chitin
a (Å)	4.52	4.70	4.66
b (Å)	18.28	17.68	8.80
c (Å)	10.28	10.53	10.33
α (°)	90.00	90.00	90.00
β (°)	90.00	90.00	90.00
γ (°)	90.00	90.00	94.76
Polarization (C/m^2)	(0, 0, 0)	(0, 0, 0)	(0, 0, −1.87)

Table 1 Lattice parameters and calculated spontaneous polarizations of the optimized crystal structures (in the spontaneous polarization calculations, the lattice vectors *b* and *c* were oriented along the *y*- and *z*-axis, respectively).

1.4 Piezoelectric performance for freestanding β-chitin nanofiber films

As we confirmed the ferroelectric characteristics of β-chitin by experimental results and theoretical calculation, we demonstrate β-chitin has a piezoelectric property because all ferroelectric materials should exhibit the piezoelectric effect. In order to measure the piezoelectricity of β-chitin film, firstly, freestanding β-chitin film using β-chitin powder from squid pen and 1,1,1,3,3,3-hexafluoro-2-propanol (HFIP) was fabricated via centrifugal casting process as shown in Figure 1.8.[28] In general, β- to α-phase transformation of chitin materials can occur during fabrication process because α-phase chitin is more thermodynamically favorable than β-phase chitin. However, the centrifugal force during centrifugal casting process has the effect preventing the phase transformation. As a result, the crystal phase of 35 μm thick freestanding β-chitin film remains the β-phase after fabrication process (Figure 1.9a and Figure 1.9b). It is well matched with the crystal phase of spin-casted chitin thin film. Although freestanding β-chitin film shows the high Young's modulus (1.7 GPa) compared to commercial PVDF film (0.7 GPa), the chitin films (~ 35 μm thick, (6 × 10) cm^2) were smooth and homogeneous, and transmitted colorful daisy scene with high flexibility and mechanical durability as shown in Figure 1.8, Figure 1.10a and Figure 1.10b.
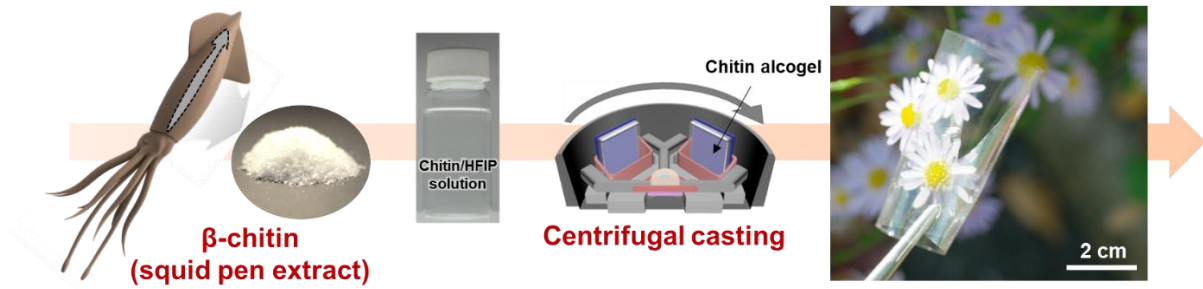
Figure 1.8 Fabrication process of piezoelectric freestanding chitin film.
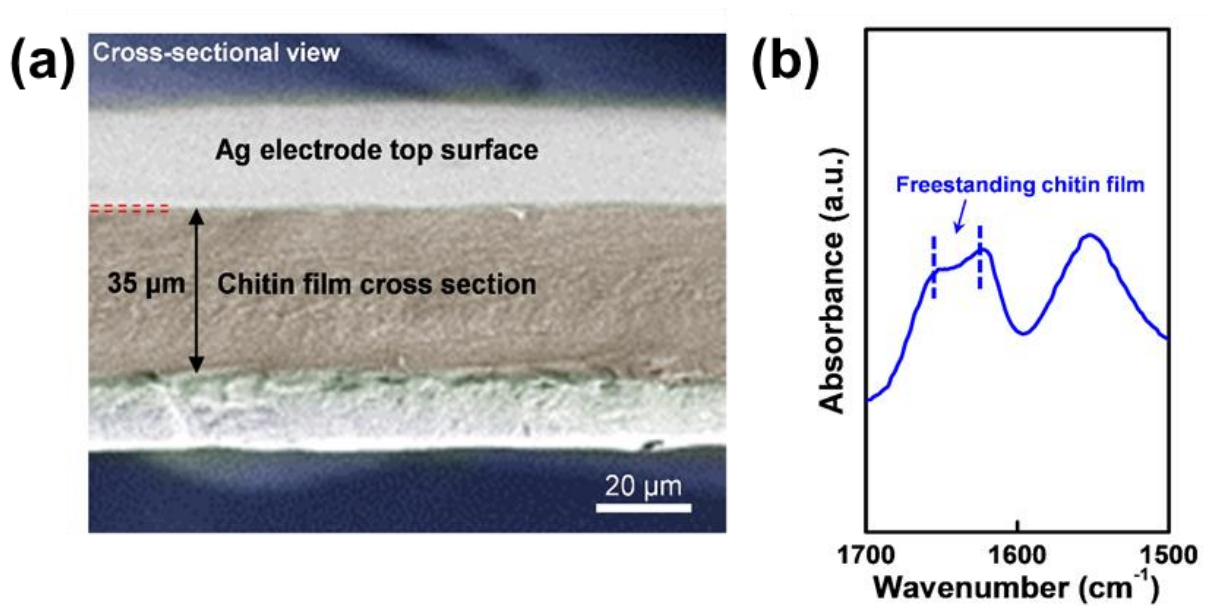
Figure 1.9 a) Cross-sectional SEM image of the freestanding chitin film. b) The FT-IR absorbance spectra of freestanding chitin film.
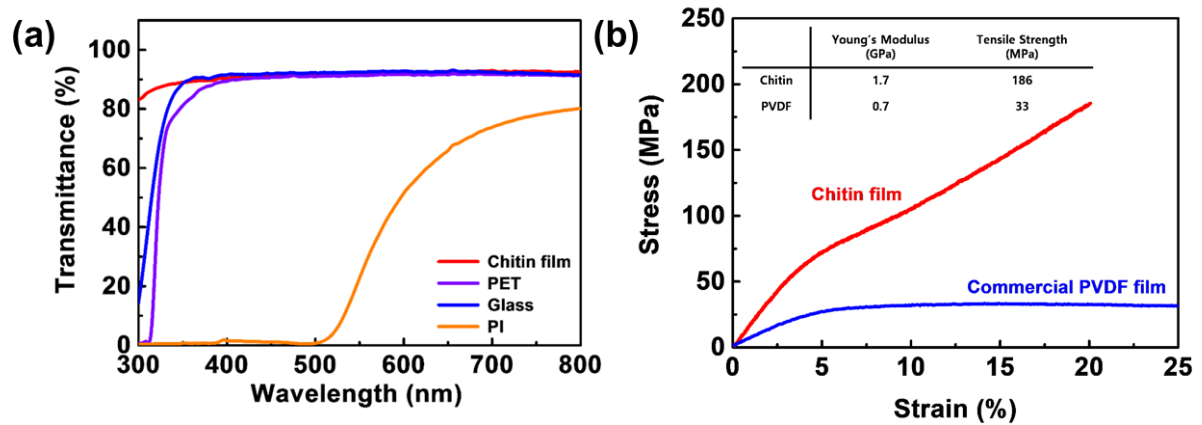
Figure 1.10 a) Transmittance spectra of freestanding chitin film (red line), PET (purple line), glass (blue line), and PI (orange line). The transmittance of freestanding chitin film is 92%. b) Stress-strain curves of chitin freestanding film (red line) and PVDF film (blue line). The extension rate is 0.1 mm/min. Inset table shows the Young's modulus and tensile strength of 35 μm thick chitin film and 80 μm thick PVDF film.

Before the piezoelectric measurement, the chitin polymer orientation in freestanding chitin film was confirmed by 2D wide angle X-ray scattering (2D WAXS). Figure 1.11 shows the result of 2D WAXS of freestanding chitin film, which shows three ring patterns at $q = 0.6$ Å^{-1}, $q = 1.3$ Å^{-1} and $q = 1.8$ Å^{-1}. The ring pattern at $q = 0.6$ Å^{-1} in 2D WAXS indicates (010) plane and two rings patterns at $q = 1.3$ Å^{-1} and $q = 1.8$ Å^{-1} represent the (100 or 002) and (003) planes. The XRD measurement demonstrates the absence of (001) and (020) plane in β-chitin.[34-35] 2D GIWAXS and WAXS analysis reveals that both *ac* plane and *bc* plane of β-chitin polymer contact the surface. The piezoelectric performance of freestanding chitin film was evaluated by applying various normal pressure and bending strain. Silver (Ag) metal electrode (100 nm) was deposited on both side of freestanding chitin film ((2 x 2) cm^2) (Figure 1.12) via DC sputtering to collect the piezoelectric charges induced by external mechanical stress. The piezoelectric output current density and voltage show 177 nA/cm^2 and 1.04 V under the normal pressure up to 100 kPa in Figure 1.13a. In particular, the piezoelectric output values rapidly increase below 10 kPa. On the other hand, α-chitin film
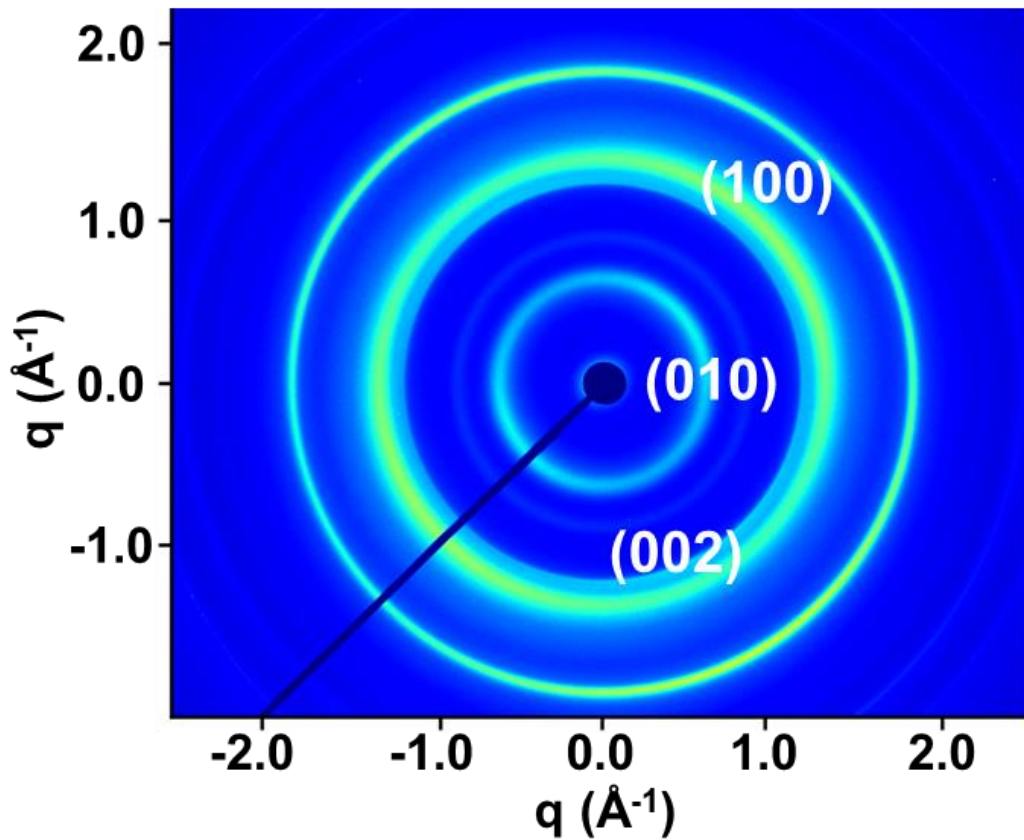
Figure 1.11 2D WAXS pattern of the freestanding chitin film. The three intensified Debye–Scherrer reflections are assigned to (010), (002) and (100) planes.
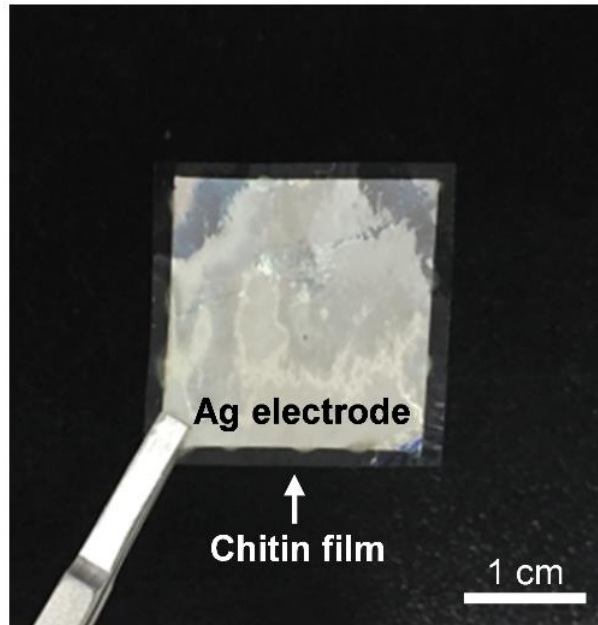
Figure 1.12 Photographic image of freestanding chitin film with Ag electrode (100 nm) on both sides.

Showed negliable piezoelectric performance compared to β-chitin film under normal pressure at 98 kPa, which indicates β-crystal phase of chitin is a critical role to generate the piezoelectric potential as shown in Figure 1.13b. The piezoelectric characteristics of chitin film with various external load resistance show in Figure 1.14. The output voltage and power density increase up to 1.7 V and 110 nW/cm² as elevating the load resistance to 10^9 Ω.
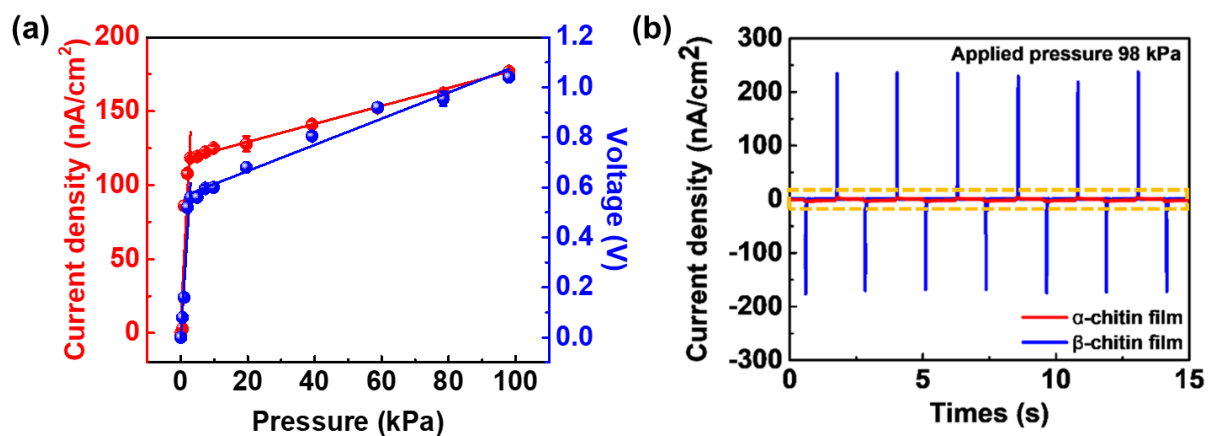
Figure 1.13 Plots of a) output current density (red dotted line) and voltage (blue dotted line) versus input pressure. Inset shows the linear sensitivity of the current density and voltage in the low-pressure regime (< 10 kPa). b) Output current density from α- (red) and β- (blue) chitin film under the consecutive normal pressure of 98 kPa.
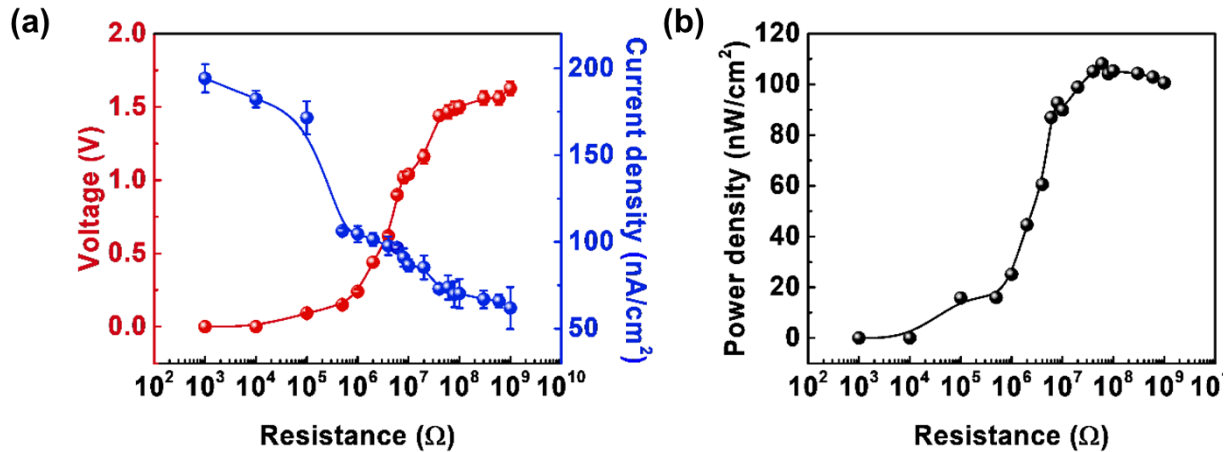
Figure 1.14 Piezoelectric characteristics of chitin film as a function of external load resistance. a) Output voltage, current density, and b) power density of chitin films with elevating external load from 10^3 to 10^9 Ω by using the vertical loading pressure of 100 kPa.

Furthermore, it was observed that the chitin film maintained the mechanical stability over 5000 cycles with a normal pressure of 100 kPa (Figure 1.15). The piezoelectric responses of bending stimuli motion also were observed by varying the bending radius. As shown in Figure 1.16, the piezoelectric responses exhibit the same tendency of the case of normal pressure event. The piezoelectric output current densities and voltage were increased up to 28 nA/cm^2 and 0.4 V, respectively.
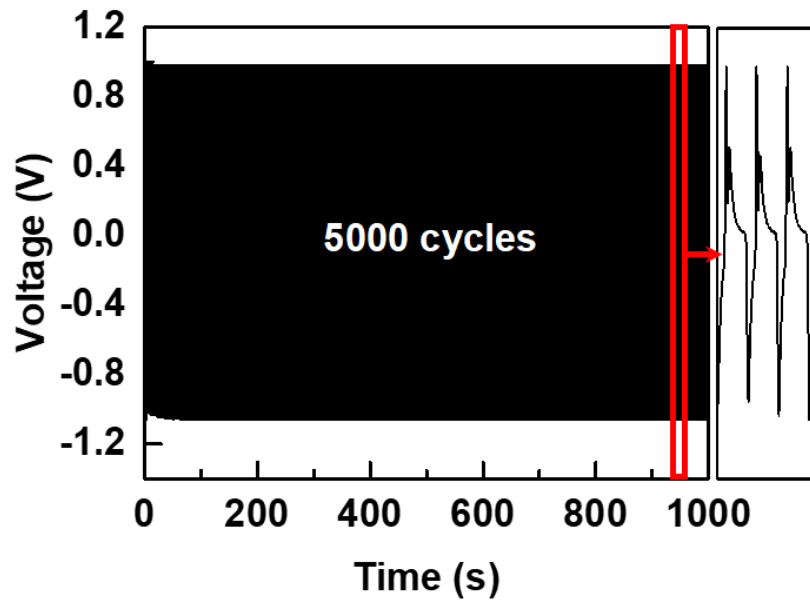
Figure 1.15 Mechanical durability of the freestanding chitin film over 5,000 times of cyclic pushing motion (100 kPa) and the corresponding output voltage signals.

Figure 1.16 a) Output current densities and b) voltage of the freestanding chitin film under the bending stimuli motion.

24
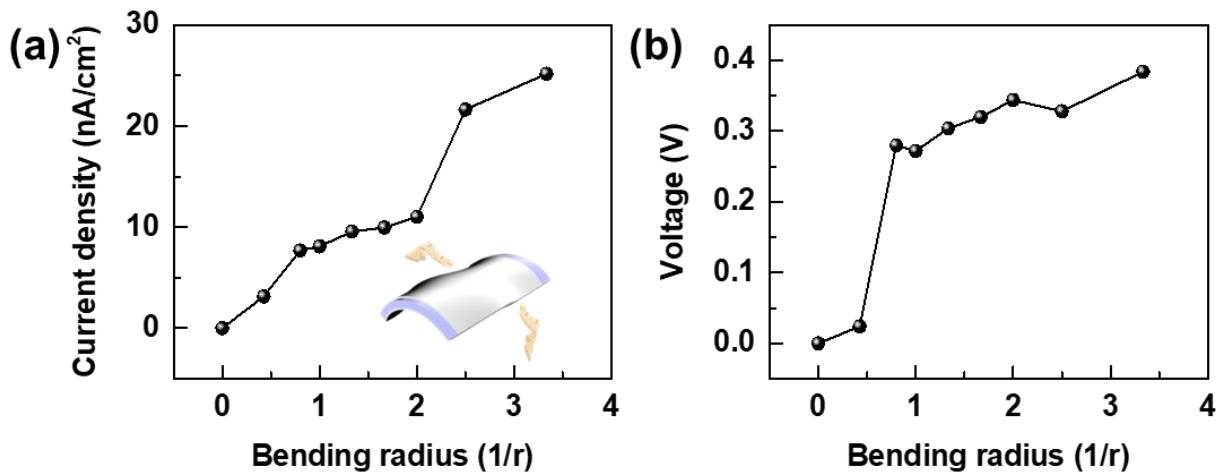
Chapter 2

2. Biodegradable piezoelectric transducers using freestanding β-chitin nanofiber films

2.1 Piezoelectric speaker and microphone for β-chitin nanofiber films

The piezoelectric materials have the reverse piezoelectric effect that is the generation of mechanical vibration when an electric energy is applied. In recent years, the reverse piezoelectric effect of piezoelectric materials has been attracted for piezoelectric actuator and transducer. PVDF and PVDF-TrFE, fluorine-based piezoelectric polymers, have been developed for the flexible piezoelectric speaker with the advantages of optical transparency, high flexibility and speaker performance. Flexible and transparent PVDF piezoelectric speaker with silver nanowires (AgNWs) was investigated by Xu et al[36] and Bae et al[37] demonstrated the flexible PVDF-TrFE speaker with graphene electrodes. Despite these many advantages of fluorine-based piezoelectric polymers, the toxic characteristic is the serious shortage as mentioned above. For this reason, eco-friendly piezoelectric biopolymers have been attracted for the development of eco-friendly piezoelectric transducer. In 2011, piezoelectric cellulose electro-active (EAPap) paper for flexible paper was evaluated by Kim et al.[38] Based on these research trends, our chitin film also have been studied for the characteristics of piezoelectric transducer. In order to investigate the performance of piezoelectric speaker for our chitin film, Ag electrodes (100 nm) were deposited on the both sides of large-scale chitin film ((4 x 6) cm^2) and the edge side was fixed by acrylic panel with Cu foil in Figure 2.1.
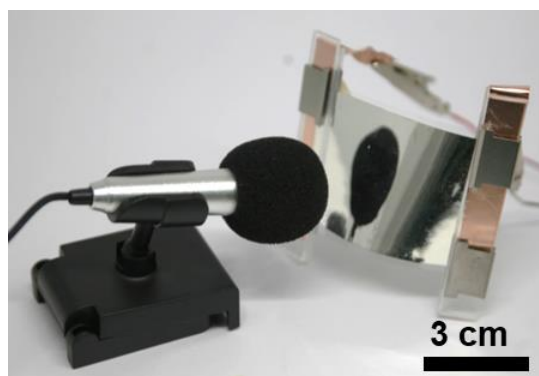
Figure 2.1 Digital photographic image of the chitin acoustic actuator ((4 x 6) cm^2) with Ag electrodes on both sides.

And then, the electronic circuit of the chitin speaker with sound source, amplifier and chitin speaker was configured in Figure 2.2. A reliable pressure response property of chitin film in the wide vibration frequency range allows us to apply in acoustic actuators and sensors. The results clearly showed actuation performance of ~ 60 dB at 20 kHz from the freestanding chitin film by monitoring the sound pressure level (SPL) response as a function of applied frequency as shown in Figure 2.3.[39] The SPL results revealed about 60 dB at 20 kHz, which are comparable performance with other piezoelectric polymers.[23, 37, 40]
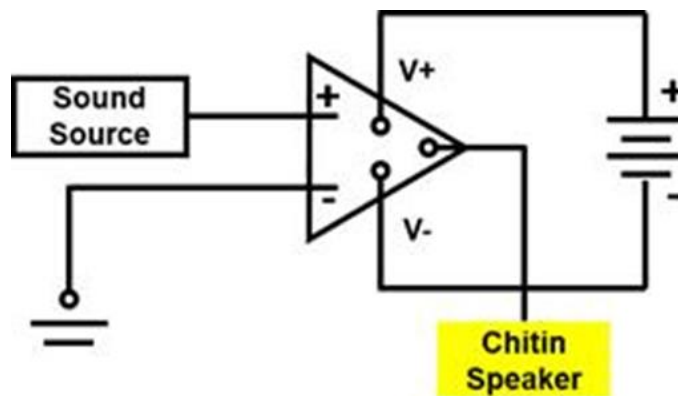
Figure 2.2 The chitin speaker electrical circuit consisting of sound source, amplifier, and piezoelectric chitin speaker.
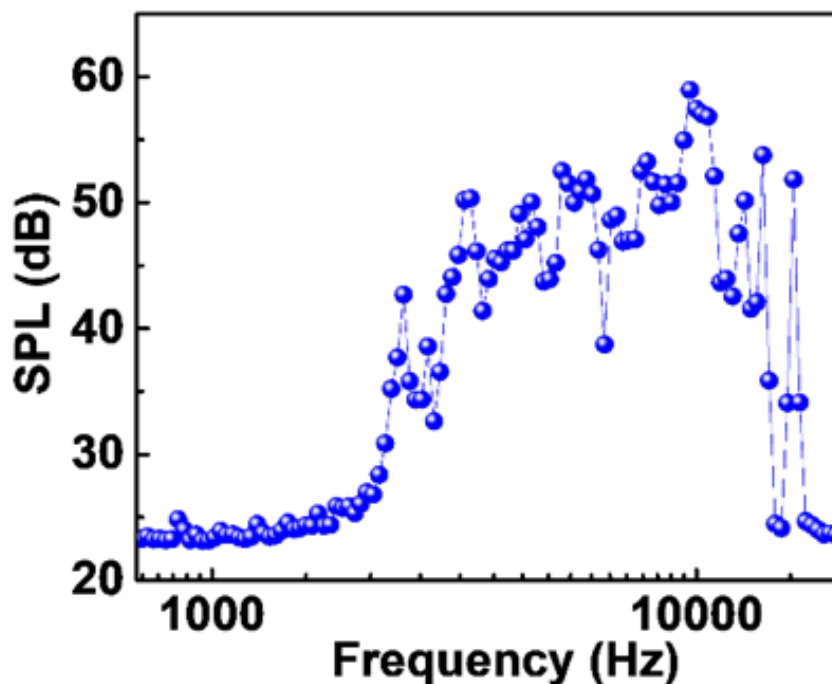
Figure 2.3 Sound pressure level (SPL) spectrum of chitin speaker in the frequency range of 300–20000 Hz.

Moreover, the piezoelectric chitin material can register a sound from the input acoustic pressure; when discrete frequencies (ranging from 100 to 1000 Hz) were fed into the predefined SPL in the open system, distinct peaks appeared in the fast Fourier transform (FFT) spectrogram. The frequencies of these peaks also corresponded to the input sound frequencies in Figure 2.4. These results suggest that the chitin film can be facilitated for the microphone and sound detector.
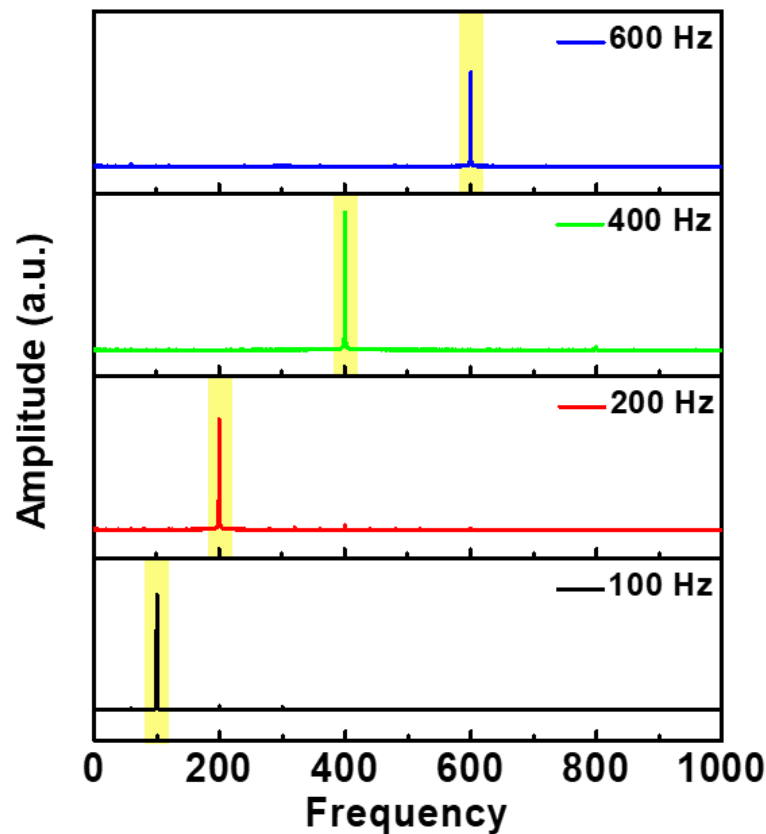
Figure 2.4 Fast Fourier transform (FFT) spectra of time-dependent piezoelectric voltage signals.

For the demonstration for the characteristics of chitin film-based piezoelectric transducer, the sound source of "Paganini Caprice no. 24" was applied to the large-scale chitin film with Ag electrodes. The sound source from the chitin speaker was recorded by commercial record

system. And then, this sound was re-recorded by the chitin microphone as the description in Figure 2.5a. The time-dependent variation with sound wave forms in the short-time Fourier transform (STFT) spectrograms in Figure 2.5b show that the sound waveforms of the chitin speaker and microphone were well matched with original sound.[41] The synchronization of STFT patterns between the original and chitin speaker was approximately 70% (Figure 2.6).
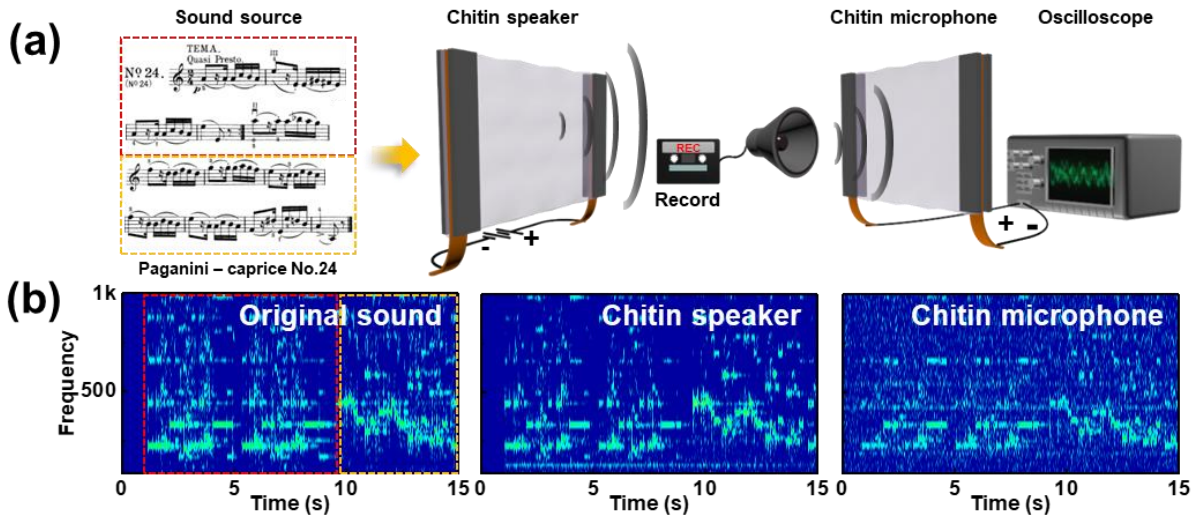
Figure 2.5 a) Schematic illustrations of the piezoelectric chitin transducer b) The short-time Fourier transform (STFT) spectrograms from the analysis of voltage variations of the original sound source, chitin speaker, and chitin microphone based on the playing music with 'Paganini Caprice NO. 24'.
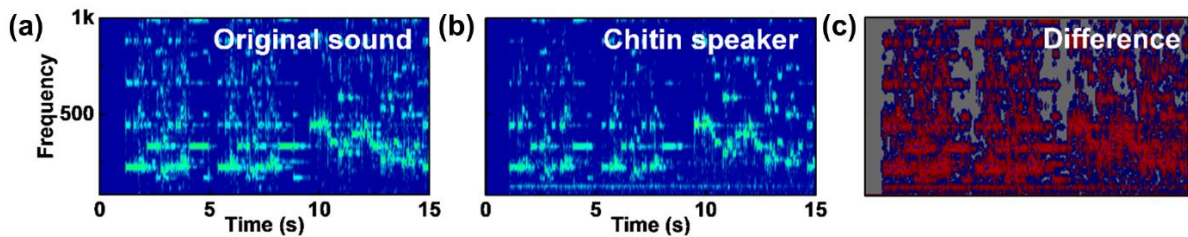
Figure 2.6 STFT patterns of a) the original sound and b) chitin speaker with 'Paganini Caprice NO. 24'. c) The difference of STFT patterns between the original sound and the STFT pattern of the chitin speaker (synchronization of 70%). The blue color indicates the difference between two images.

We further extend the utilization of our chitin film to a transparent and flexible speaker combined with AgNWs as the top and bottom electrodes (Figure 2.7). The high optical transmittance (71%) with decent conductivity (approximately $50\,\Omega$/square) of the AgNWs/PMMA/chitin/PMMA/AgNWs layer enabled to resemble the original sound modulation in the STFT spectrogram, demonstrating the excellent potentials of the chitin transducer as a high-quality speaker (Figure 2.8). It is noted that the device was fabricated with PMMA layers, which protect the chitin film from the water-based AgNWs solution, but negligibly affect the sound quality of the transducer.
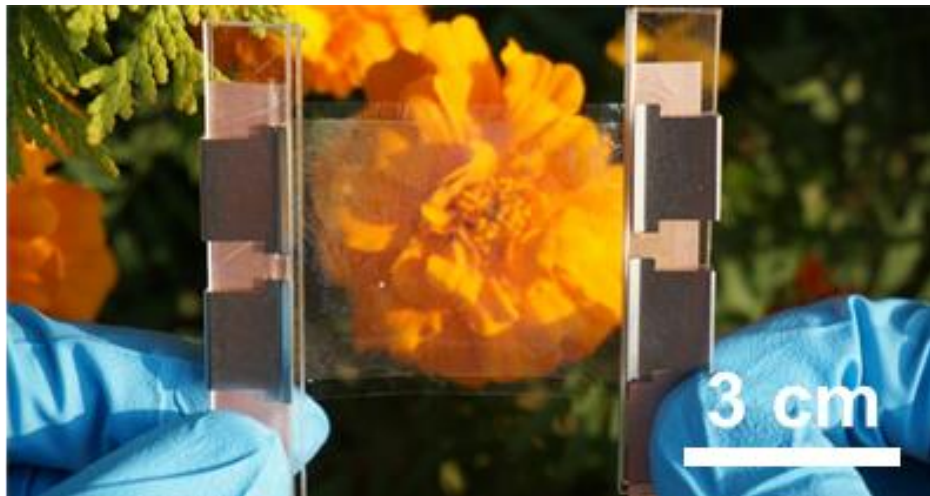
Figure 2.7 Digital photograph of the transparent chitin speaker sandwiched between two AgNWs electrodes.
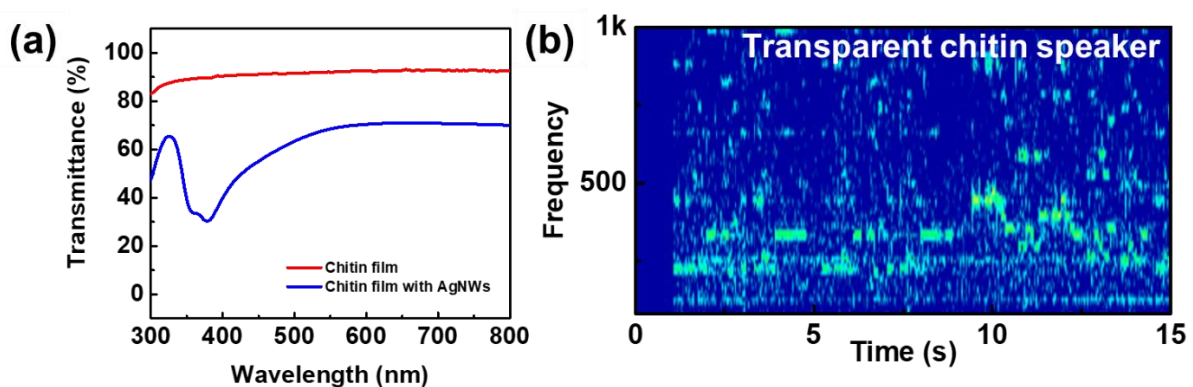
Figure 2.8 a) Transmittance spectra of freestanding chitin film with (blue line) and without (red line) AgNWs electrodes on both sides. b) STFT signals of the transparent chitin speaker, verifying the high-quality sound performance of the transparent chitin speaker.

2.2 Biodegradation for chitin films

The particular advantages of our chitin film is environment-friendly characteristic that are biodegradable in chitinase enzyme dissolved in water. The time-lapse photographic images and illuistations in Figure 2.9 show our biodegradable chitin film was gradually degraded in chitinased solution (1 UN/10ml) withtin eight days. During the biodegradation process, the non-toxic byproducts which are acetate, N-acetylglucosamine (GlcNAc), glucosamine (GlcN), glucose (Glc) and CO_2, were generated.[42]
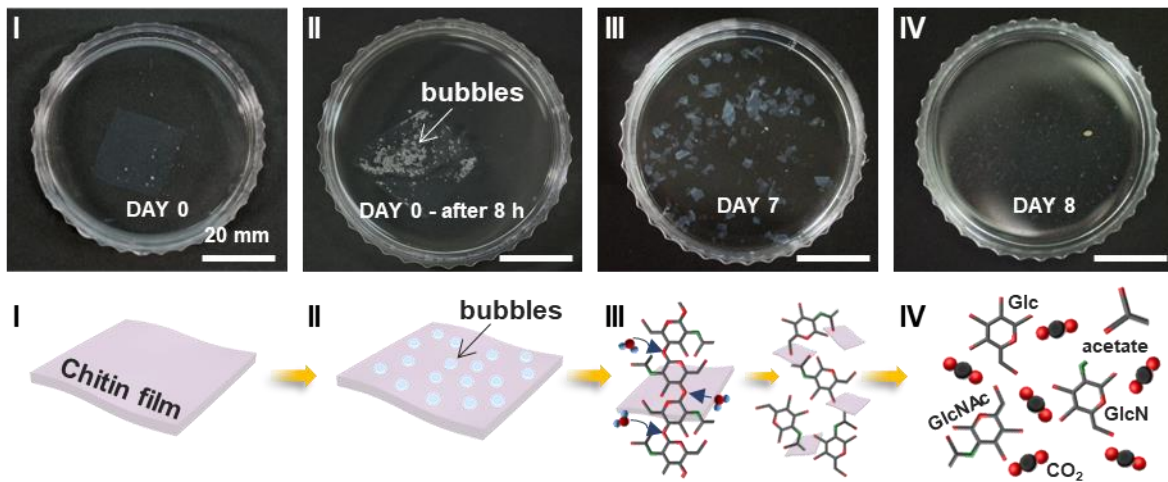
Figure 2.9 Series photographs and schematic illustrations of corresponding stages of biodegradation process in chitinase solution (1 UN/10ml).
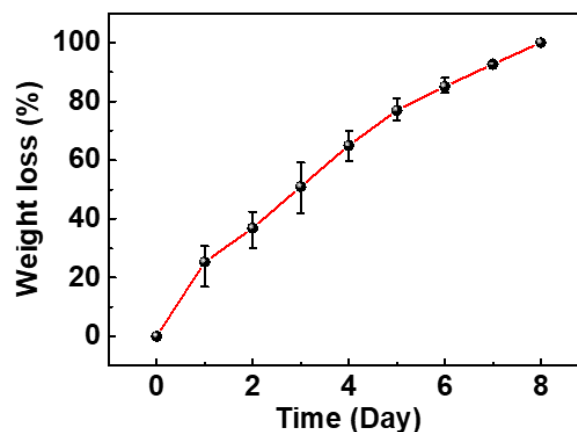
Figure 2.10 Plots of the weight loss of the chitin film as a function of time in chitinase solution (1 UN/10ml).

The weight of chitin film in chitinase solution also gradually decreased as shown in Figure 2.10. Moreover, we were able to control the degradation time by adjusting the chitinase solution concentration. In Figure 2.11, the degradation time of the chitin film decreased to 4 days at high chitinase solution concentration (5 UN/10ml).
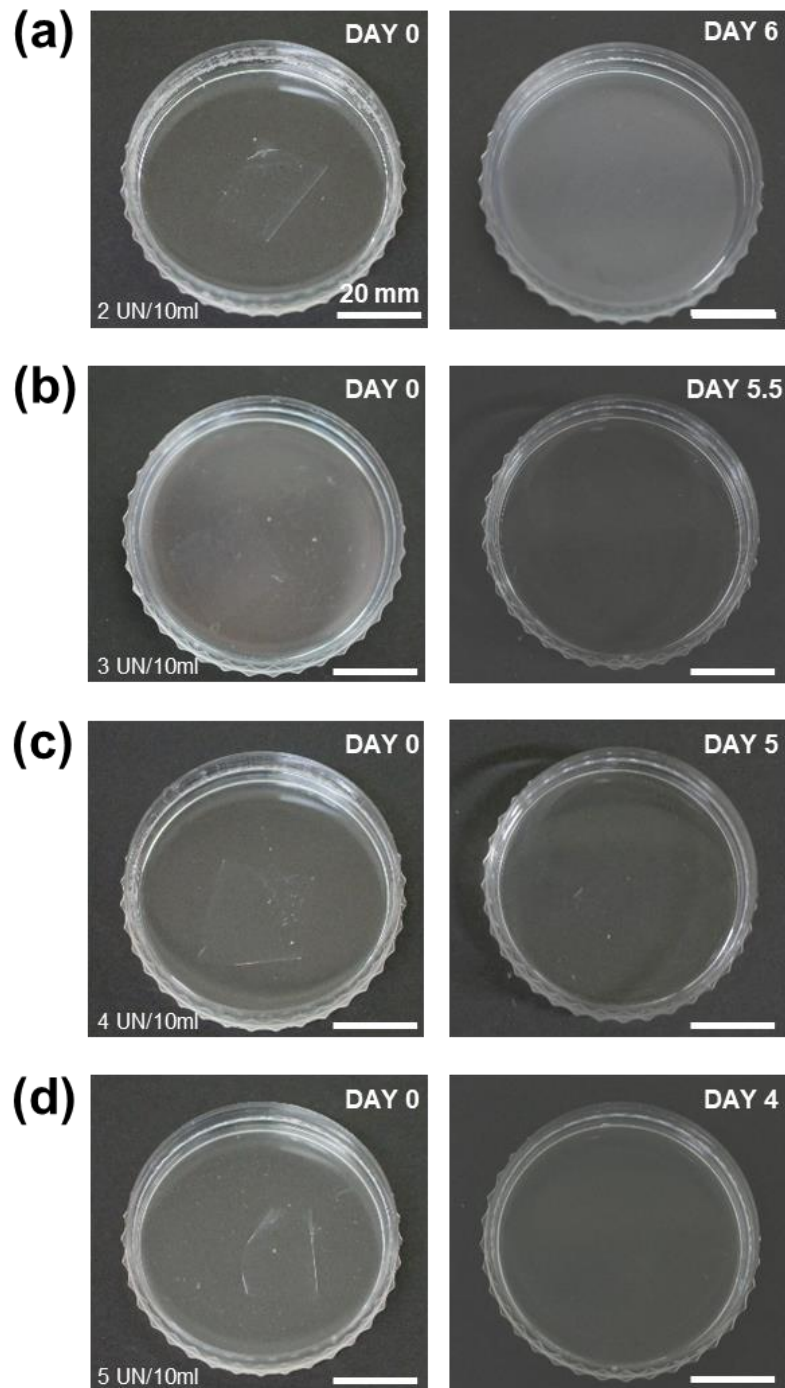
Figure 2.11 A digital photograph of biodegradation of the chitin film by chitinase solution a) 2 UN/10ml, b) 3 UN/10ml, c) 4 UN/10ml, and d) 5 UN/10ml as time advanced.

In particular, during the degradation process of our chitin film in the stage II in Figure 2.9, gas bubbles generation was observed. For the qualitatively gas analyis during the degradation process, a home-built differencial electrochemical mass spectrometry (DEMS) system was monitored with Ar carrier gas injection (Figure 2.12a).[43] As shown in Figure 2.12b, only CO_2 gas was evolved after 18 hours chitin film immersion in chitinase solution. It suggested that our chitin film is suitable for the eco-fiendly piezoelectric materials with non-toxic byproduct during degradation process.
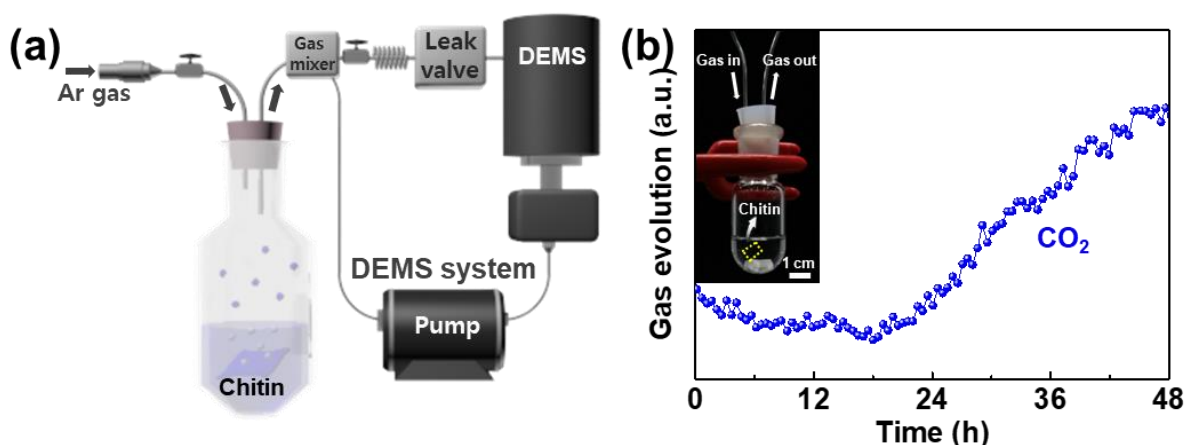
Figure 2.12 a) Schematic illustrations of home-built DEMS system. b) The consecutively measured CO_2 signals of chitin film in chitinase solution. The CO_2 evolution is detected after 18 hours and monotonically increased until the end of the measurement. The inset shows a photographic image of chitin film immersed in chitinase solution.

2.3 Experimental section

2.3.1 Freestanding chitin film fabrication

Squid pen β-chitin powder was extracted following a conventional protocol, and dissolved in 1,1,1,3,3,3-hexafluoro-2-propanol (HFIP) (Halocarbon, USA) solvent (0.4% w/v)[44]. Sixty-milliliters of the chitin/HFIP solution was poured into a rectangular polypropylene plate sized ((12.5×9) cm^2). The chitin/HFIP alcogel was fabricated as described in previous work. The alcogel-containing polypropylene plate was centrifugal-casted (2100 rpm for 3 h) in a large-capacity multipurpose centrifuge (Combi-514R, Hanil Science Inc., Korea) at room temperature. The centrifugal-casted freestanding chitin film was sandwiched between two glass plates, each treated with trichloro(octadecyl)silane (OTS)

(Sigma-Aldrich, Korea). The assembly was processed in a vacuum hot press machine at 120 °C for 2 h for calendaring of the freestanding chitin film.[28]

2.3.2 Chitin piezoelectric transducers fabrication

To form uniform electrodes on the chitin piezoelectric devices, a 100 nm-thick silver (Ag) was deposited on the freestanding chitin film by a DC magnetron sputtering system operated at 700 W (SRN-120, SORONA, Korea) and 10^{-7} Torr. For the chitin pressure sensor, the edge of the Ag-coated freestanding chitin film was attached to the copper (Cu) wires using silver paste. For the chitin acoustic actuator, the edge of the Ag-coated chitin freestanding film ((4 × 6) cm^2) was fixed to Cu foil ((1 × 4) cm^2) using a rectangular acrylic panel. To fabricate the transparent chitin acoustic actuator, poly methyl methacrylate (PMMA) (Micro Chem, USA) was spin-coated (1000 rpm for 1 min) on both sides of the freestanding chitin film ((4 × 6) cm^2), forming a protective layer against the water-based solution of silver nanowires (AgNWs) (C3Nano, USA). The assembly was then annealed at 85 °C for 10 min. Next, the transparent AgNWs electrodes (0.3 wt%; average length and diameter 15 µm and 20 nm, respectively) were made by spin-coating (900 rpm for 1 min) both sides of the PMMA-coated freestanding chitin film. Finally, the AgNWs-coated transparent chitin film was dried overnight in a vacuum oven maintained at room temperature.

2.3.3 Freestanding chitin film in vitro biodegradation

The chitin film was immersed in 1 UN/10 ml chitinase extracted from Streptomyces griseus (Sigma-Aldrich, Korea). The chitinase was dissolved in D.I. water at room temperature. The degradation extent of the film was expressed as the weight-loss ratio. To calculate the weight loss as a function of degradation time, we recorded the initial weight of the chitin film. As the chitin film degraded, the weight of the remaining film was measured daily until the degradation was complete. During the degradation process, the gas evolution was monitored by a home-built differential electrochemical mass spectrometry (DEMS) system.

2.3.4 Characterizations

Non-contact mode AFM was performed on an XE-100 with PPP-NCHR non-contact cantilevers (Park systems, Korea). The prepared chitin film was analyzed in FTIR-ATR mode by a NICOLET iS 50 (Thermo scientific, Korea) in the wavenumber range 650–4000 cm^{-1}.

2D GIWAXS and WAXS were performed on the 6D UNIST-PAL line at the Pohang Accelerator Laboratory (Pohang University of Science and Technology, Korea). The chitin thin film was irradiated with monochromatized X-rays ($\lambda = 0.106879$ nm) at a grazing incidence angle of 0.13°. The ferroelectric and dielectric properties of the chitin thin film were measured in a virtual ground circuit (Radiant Technologies, Precision LC unit) and capacitance voltage unit (Keithley 4210), respectivel. Cross-sectional SEM images of the freestanding chitin film between the top and bottom Ag electrodes was obtained by a JSM-7600F (JEOL, Japan) with an acceleration voltage of 5 kV. To increase the contrast in the SEM imaging, a thin Pt layer was deposited on the freestanding chitin film using a CRESSINGTON sputter coater Q108 (Cressington Scientific Instruments, UK). Parallel transmittance was measured in a dark box with an AvaLight-DHc light source and an AvaSpec-2048L detector (AVANTES, USA). The output current and voltage induced by the generated piezoelectric potential were respectively measured by a sourcemeter (2450-SCPI, Keithley, USA) and an oscilloscope (DPO 2022B, Tektronix, USA) at zero-bias, using a two-probe method with Cu wires connected to the top and bottom of the Ag electrodes on the freestanding chitin film. Mechanical stress was applied on the freestanding chitin film by a pushing tester (JIPT-100, JUNIL TECH, Korea), which provided static, high-frequency dynamic pressures. The bending strain was applied by a bending machine (JIPT-200, JUNIL TECH, Korea). The chitin acoustic actuator performance was measured by the sound pressure level (SPL). The chitin acoustic actuator generated 300–20000 Hz sound, which was detected by a normal microphone in an anechoic room. To verify the sound-detection ability of the freestanding chitin film, the sound frequency was controlled by a commercial speaker and the corresponding piezoelectric output voltage was measured by an oscilloscope (DPO 2022B, Tektronix, USA). In the sound-detection measurements, the chitin microphone and commercial speaker were separated by 1 cm.

2.3.5 Computer simulation

Spin-polarized DFT calculations were performed in the Vienna Ab-initio Simulation Package (VASP).[32-33] The exchange correlation potential of the electrons was determined by the generalized gradient approximation using the Perdew–Burke–Ernzerhof (GGA-PBE) functional.[45] The electron–ion interactions were described by the standard projector augmented wave potentials,[46-47] treating the 1s state of H and the 2s and 2p states of C, N,

and O as the valence states. The wave functions were expanded as a plane-wave basis set with an energy cutoff of 600 eV. The van der Waals interactions were corrected by Grimme's D2 method.[48] The convergence criterion for the electronic self-consistency loop was set to 10^{-8} eV. The lattice parameters and atomic positions were fully relaxed under crystallographic symmetry until the Hellmann–Feynman forces fell below 0.01 eV/Å. The Brillouin zone integration was performed on a (5 × 1 × 3) k-point grid for the α-chitin unit cell, and on a (5 × 3 × 3) k-point grid for the β-chitin unit cell. The crystal structures of α- and β-chitin were taken from Sikorski et al[49] and Sawada et al.[50], respectively. For α-chitin, we considered two distinctive conformations of the hydroxymethyl group (i.e., O6A and O6B), which were experimentally revealed by Sikorski et al. The spontaneous polarization of a periodic polymeric crystal was computed by the Berry Phase approach.[51] The lattice parameters and the calculated spontaneous polarization of the optimized crystal structures are tabulated in Table 1.

2.4 Conclusions

In conclusion, we demonstrated the piezoelectricity in crystalline β-rich chitin materials. In our chitin thin film prepared by the spin casting method enabled to measuring the appropriate ferroelectric polarization in an electric field and confirmed the molecular polarization by GIXD measurements with the support of theoretical calculations. The strong piezoelectric characteristics of the chitin film yielded a respectable output current density of $177\,nA/cm^2$ and reliable endurance performance (5000 cycles of a 100 kPa vertical pressure). We further demonstrated a paper-type acoustic actuator and sensor using a large-area chitin film that operates over a wide range of SPL, with good response to harmonic frequencies. The optically transparent AgNWs electrodes actualized a transparent chitin speaker with respectable sound quality. Finally, under the optimized condition, the chitin material was digested by chitinase enzyme with no generation of toxic residues. Finally, we remark that the piezoelectric chitin is a promisingly new biodegradable transducer material and will actively promote researches on eco-friendly piezoelectric materials.

References

1. Curie, J., Developpement par compression de l'electricite polaire dans les cristaux hemiedres a faces inclinees. *Bull. Soc. Fr. Mineral.* **1880,** *3*, 90.

2. Rogers, J. A.; Someya, T.; Huang, Y., Materials and Mechanics for Stretchable Electronics. *Science* **2010,** *327* (5973), 1603-1607.

3. Ru, F. F.; Wei, T.; Lin, W. Z., Flexible Nanogenerators for Energy Harvesting and Self-Powered Electronics. *Advanced Materials* **2016,** *28* (22), 4283-4305.

4. Takei, K.; Takahashi, T.; Ho, J. C.; Ko, H.; Gillies, A. G.; Leu, P. W.; Fearing, R. S.; Javey, A., Nanowire active-matrix circuitry for low-voltage macroscale artificial skin. *Nature Materials* **2010,** *9*, 821.

5. Park, J.; Kim, M.; Lee, Y.; Lee, H. S.; Ko, H., Fingertip skin–inspired microstructured ferroelectric skins discriminate static/dynamic pressure and temperature stimuli. *Science advances* **2015,** *1* (9), e1500661.

6. Jaffe, B., *Piezoelectric ceramics*. Elsevier: 2012; Vol. 3.

7. Jihye, K.; Hwan, L. J.; Hanjun, R.; Ju-Hyuck, L.; Usman, K.; Han, K.; Soo, K. S.; Sang-Woo, K., High-Performance Piezoelectric, Pyroelectric, and Triboelectric Nanogenerators Based on P(VDF-TrFE) with Controlled Crystallinity and Dipole Alignment. *Advanced Functional Materials* **2017,** *27* (22), 1700702.

8. Persano, L.; Dagdeviren, C.; Su, Y.; Zhang, Y.; Girardo, S.; Pisignano, D.; Huang, Y.; Rogers, J. A., High performance piezoelectric devices based on aligned arrays of nanofibers of poly(vinylidenefluoride-co-trifluoroethylene). *Nature Communications* **2013,** *4*, 1633.

9. Cha, S.; Kim, S. M.; Kim, H.; Ku, J.; Sohn, J. I.; Park, Y. J.; Song, B. G.; Jung, M. H.; Lee, E. K.; Choi, B. L., Porous PVDF as effective sonic wave driven nanogenerators. *Nano letters* **2011,** *11* (12), 5142-5147.

10. Fuh, Y.-K.; Chen, P.-C.; Huang, Z.-M.; Ho, H.-C., Self-powered sensing elements based on direct-write, highly flexible piezoelectric polymeric nano/microfibers. *Nano Energy* **2015,** *11*, 671-677.

11. Chen, D.; Sharma, T.; Zhang, J. X., Mesoporous surface control of PVDF thin films for enhanced piezoelectric energy generation. *Sensors and Actuators A: physical* **2014,** *216*, 196-201.

12. Lee, J. H.; Lee, K. Y.; Gupta, M. K.; Kim, T. Y.; Lee, D. Y.; Oh, J.; Ryu, C.; Yoo, W.

J.; Kang, C. Y.; Yoon, S. J., Highly stretchable piezoelectric-pyroelectric hybrid nanogenerator. *Advanced Materials* **2014,** *26* (5), 765-769.

13.   Pi, Z.; Zhang, J.; Wen, C.; Zhang, Z.-b.; Wu, D., Flexible piezoelectric nanogenerator made of poly (vinylidenefluoride-co-trifluoroethylene)(PVDF-TrFE) thin film. *Nano Energy* **2014,** *7*, 33-41.

14.   Xu, H.; Cheng, Z.-Y.; Olson, D.; Mai, T.; Zhang, Q.; Kavarnos, G., Ferroelectric and electromechanical properties of poly (vinylidene-fluoride–trifluoroethylene–chlorotrifluoroethylene) terpolymer. *Applied Physics Letters* **2001,** *78* (16), 2360-2362.

15.   Park, Y. J.; Kang, S. J.; Park, C.; Kim, K. J.; Lee, H. S.; Lee, M. S.; Chung, U.-I.; Park, I. J., Irreversible extinction of ferroelectric polarization in P (VDF-TrFE) thin films upon melting and recrystallization. *Applied physics letters* **2006,** *88* (24), 242908.

16.   Siddiqui, S.; Kim, D.-I.; Nguyen, M. T.; Muhammad, S.; Yoon, W.-S.; Lee, N.-E., High-performance flexible lead-free nanocomposite piezoelectric nanogenerator for biomechanical energy harvesting and storage. *Nano Energy* **2015,** *15*, 177-185.

17.   Persano, L.; Dagdeviren, C.; Su, Y.; Zhang, Y.; Girardo, S.; Pisignano, D.; Huang, Y.; Rogers, J. A., High performance piezoelectric devices based on aligned arrays of nanofibers of poly (vinylidenefluoride-co-trifluoroethylene). *Nature communications* **2013,** *4*, 1633.

18.   Nguyen, T., Degradation of poly [vinyl fluoride] and poly [vinylidene fluoride]. *Polymer Reviews* **1985,** *25* (2), 227-275.

19.   Zulfiqar, S.; Zulfiqar, M.; Rizvi, M.; Munir, A.; McNeill, I., Study of the thermal degradation of polychlorotrifluoroethylene, poly (vinylidene fluoride) and copolymers of chlorotrifluoroethylene and vinylidene fluoride. *Polymer Degradation and Stability* **1994,** *43* (3), 423-430.

20.   Fukada, E.; Sasaki, S., Piezoelectricity of α-chitin. *Journal of Polymer Science Part B: Polymer Physics* **1975,** *13* (9), 1845-1847.

21.   Ghosh, S. K.; Mandal, D., Bio-assembled, piezoelectric prawn shell made self-powered wearable sensor for non-invasive physiological signal monitoring. *Applied Physics Letters* **2017,** *110* (12), 123701.

22.   Kim, J.; Yun, S.; Ounaies, Z., Discovery of cellulose as a smart material. *Macromolecules* **2006,** *39* (12), 4202-4206.

23.   Kim, J.-H.; Yun, S.; Kim, J.-H.; Kim, J., Fabrication of piezoelectric cellulose paper and audio application. *Journal of Bionic Engineering* **2009,** *6* (1), 18-21.

24.   Fukada, E., Piezoelectricity of wood. *Journal of the Physical Society of Japan* **1955,** *10* (2), 149-154.

25.   Kim, K. N.; Chun, J.; Chae, S. A.; Ahn, C. W.; Kim, I. W.; Kim, S.-W.; Wang, Z. L.; Baik, J. M., Silk fibroin-based biodegradable piezoelectric composite nanogenerators using lead-free ferroelectric nanoparticles. *Nano Energy* **2015,** *14*, 87-94.

26.   Rajala, S.; Siponkoski, T.; Sarlin, E.; Mettänen, M.; Vuoriluoto, M.; Pammo, A.; Juuti, J.; Rojas, O. J.; Franssila, S.; Tuukkanen, S., Cellulose nanofibril film as a piezoelectric sensor material. *ACS applied materials & interfaces* **2016,** *8* (24), 15607-15614.

27.   Binetti, V. R.; Schiffman, J. D.; Leaffer, O. D.; Spanier, J. E.; Schauer, C. L., The natural transparency and piezoelectric response of the Greta oto butterfly wing. *Integrative Biology* **2009,** *1* (4), 324-329.

28.   Jin, J.; Lee, D.; Im, H. G.; Han, Y. C.; Jeong, E. G.; Rolandi, M.; Choi, K. C.; Bae, B. S., Chitin nanofiber transparent paper for flexible green electronics. *Advanced Materials* **2016,** *28* (26), 5169-5175.

29.   Kim, K.; Ha, M.; Choi, B.; Joo, S. H.; Kang, H. S.; Park, J. H.; Gu, B.; Park, C.; Park, C.; Kim, J.; Kwak, S. K.; Ko, H.; Jin, J.; Kang, S. J., Biodegradable, electro-active chitin nanofiber films for flexible piezoelectric transducers. *Nano Energy* **2018,** *48*, 275-283.

30.   Ogawa, Y.; Lee, C. M.; Nishiyama, Y.; Kim, S. H., Absence of Sum Frequency Generation in Support of Orthorhombic Symmetry of α-Chitin. *Macromolecules* **2016,** *49* (18), 7025-7031.

31.   Rinaudo, M., Chitin and chitosan: properties and applications. *Progress in polymer science* **2006,** *31* (7), 603-632.

32.   Kresse, G.; Furthmüller, J., Efficient iterative schemes for ab initio total-energy calculations using a plane-wave basis set. *Physical review B* **1996,** *54* (16), 11169.

33.   Kresse, G.; Furthmüller, J., Efficiency of ab-initio total energy calculations for metals and semiconductors using a plane-wave basis set. *Computational materials science* **1996,** *6* (1), 15-50.

34.   Nagahama, H.; Higuchi, T.; Jayakumar, R.; Furuike, T.; Tamura, H., XRD studies of β-chitin from squid pen with calcium solvent. *International journal of biological macromolecules* **2008,** *42* (4), 309-313.

35.   Noishiki, Y.; Takami, H.; Nishiyama, Y.; Wada, M.; Okada, S.; Kuga, S., Alkali-induced conversion of β-chitin to α-chitin. *Biomacromolecules* **2003,** *4* (4), 896-899.

36.	Xu, S.; Man, B.; Jiang, S.; Liu, M.; Yang, C.; Chen, C.; Zhang, C., Graphene–silver nanowire hybrid films as electrodes for transparent and flexible loudspeakers. *CrystEngComm* **2014,** *16* (17), 3532-3539.

37.	Bae, S.-H.; Kahya, O.; Sharma, B. K.; Kwon, J.; Cho, H. J.; Ozyilmaz, B.; Ahn, J.-H., Graphene-P (VDF-TrFE) multilayer film for flexible applications. *ACS nano* **2013,** *7* (4), 3130-3138.

38.	Kim, J.; Yun, G.-Y.; Kim, J.-H.; Lee, J.; Kim, J.-H., Piezoelectric electro-active paper (EAPap) speaker. *Journal of mechanical science and technology* **2011,** *25* (11), 2763-2768.

39.	Li, W.; Torres, D.; Díaz, R.; Wang, Z.; Wu, C.; Wang, C.; Wang, Z. L.; Sepúlveda, N., Nanogenerator-based dual-functional and self-powered thin patch loudspeaker or microphone for flexible electronics. *Nature Communications* **2017,** *8*, 15310.

40.	Xu, S.; Man, B.; Jiang, S.; Chen, C.; Yang, C.; Liu, M.; Gao, X.; Sun, Z.; Zhang, C., Flexible and transparent graphene-based loudspeakers. *Applied Physics Letters* **2013,** *102* (15), 151902.

41.	Kang, D.; Pikhitsa, P. V.; Choi, Y. W.; Lee, C.; Shin, S. S.; Piao, L.; Park, B.; Suh, K.-Y.; Kim, T.-i.; Choi, M., Ultrasensitive mechanical crack-based sensor inspired by the spider sensory system. *Nature* **2014,** *516* (7530), 222.

42.	Beier, S.; Bertilsson, S., Bacterial chitin degradation—mechanisms and ecophysiological strategies. *Frontiers in microbiology* **2013,** *4*, 149.

43.	Kang, S. J.; Mori, T.; Narizuka, S.; Wilcke, W.; Kim, H.-C., Deactivation of carbon electrode for elimination of carbon dioxide evolution from rechargeable lithium–oxygen cells. *Nature communications* **2014,** *5*, 3937.

44.	Chaussard, G.; Domard, A., New aspects of the extraction of chitin from squid pens. *Biomacromolecules* **2004,** *5* (2), 559-564.

45.	Perdew, J. P.; Burke, K.; Ernzerhof, M., Generalized gradient approximation made simple. *Physical review letters* **1996,** *77* (18), 3865.

46.	Blöchl, P. E., Projector augmented-wave method. *Physical review B* **1994,** *50* (24), 17953.

47.	Kresse, G.; Joubert, D., From ultrasoft pseudopotentials to the projector augmented-wave method. *Physical Review B* **1999,** *59* (3), 1758.

48.	Grimme, S., Semiempirical GGA-type density functional constructed with a long-range dispersion correction. *Journal of computational chemistry* **2006,** *27* (15), 1787-1799.

49.   Sikorski, P.; Hori, R.; Wada, M., Revisit of α-chitin crystal structure using high resolution X-ray diffraction data. *Biomacromolecules* **2009,** *10* (5), 1100-1105.

50.   Sawada, D.; Nishiyama, Y.; Langan, P.; Forsyth, V. T.; Kimura, S.; Wada, M., Direct determination of the hydrogen bonding arrangement in anhydrous β-chitin by neutron fiber diffraction. *Biomacromolecules* **2011,** *13* (1), 288-291.

51.   King-Smith, R.; Vanderbilt, D., Theory of polarization of crystalline solids. *Physical Review B* **1993,** *47* (3), 1651.